Magnetic Response of Single-Walled Carbon Nanotubes Induced by an External Magnetic Field

Mikhail Kibalchenko,[†,*] Mike C. Payne,[†] and Jonathan R. Yates[‡]

[†]TCM Group, Cavendish Laboratory, University of Cambridge, Cambridge, CB3 0HE, United Kingdom, and [‡]Department of Materials, University of Oxford, Oxford, OX1 3PH, United Kingdom

ABSTRACT Using first-principles density functional calculations, magnetically induced currents are obtained for zigzag single-walled carbon nanotubes. Clear differences and trends in current flow are observed between the different nanotube families. In particular, for a magnetic field applied along the tube axis, the current response of the $\lambda = 0$ infinite nanotubes is paramagnetic, whereas for $\lambda = 1$ and 2 nanotubes, the response is diamagnetic. The results are used to predict and interpret the significant changes in NMR properties for small molecules encapsulated inside a tube.

KEYWORDS: carbon nanotubes · nuclear magnetic resonance · magnetically induced currents · nucleus-independent chemical shift · density functional theory · first-principles · molecule encapsulation

Carbon nanotubes have been under extensive experimental and theoretical study for the past decade as a result of their unusual and potentially useful properties. Recent advances to accurately characterize a given sample of nanotubes[1] and progress in nanotube sorting[2] have refocused research efforts in technological exploitation of carbon nanotubes. One area of such research efforts has focused on the encapsulation of molecules inside carbon nanotubes.[3] The environment inside an ideal nanotube is thought to be a potential well where molecules would be easily encapsulated after overcoming a small energy barrier on entry.[4] It is also a relatively inert environment[5,6] that would reduce bonding to the nanotube wall. The curvature of the nanotube wall is the reason for reduced reactivity on the interior of a carbon nanotube as opposed to the exterior. The strain energy has been shown to decrease on covalent bonding of an atom to the exterior but increase if the bonding was on the interior of the nanotube wall.[7] Encapsulation of molecules inside nanotubes is now becoming routine with studies examining encapsulation of hydrogen,[8] metal halides,[9] and larger molecules, such as Buckminster fullerenes,[10] DNA,[11] and even proteins.[12]

One technological application of molecule encapsulation is drug delivery.[13−16] For example, encapsulation of anticancer drugs[17,18] or collagen-like peptides[19] has been proposed. To aid this type of application, it is important to have spectroscopic techniques that can provide information on the structure and environment of the molecule encapsulated within the tube. Solid-state nuclear magnetic resonance (NMR) is a useful spectroscopic tool for such studies whereby the chemical shifts of the encapsulated molecules can be measured. Carbon nanostructures present a challenge to NMR experiments due to the impurity of samples and the presence of residual catalyst. However, with careful sample preparation, it is now possible to obtain ^{13}C spectra with relatively narrow resonances.[20,21] Very recently, NMR measurements have been made from samples encapsulated within nanotubes.[22] The differences in chemical shifts between the encapsulated molecule and the free molecule have the potential to provide information on how the molecule's structure changes on encapsulation as well as the environment experienced by the molecule inside the nanotube. However, such experimental results would be complicated by the screening effects of currents within the nanotube itself. The induction of currents and the magnetic response of carbon nanotubes is a major subject of interest in itself and has been widely discussed.[23,24]

In this paper, we examine the magnetic response of zigzag single-walled nanotubes (SWNTs) and show that the chemical shifts of the encapsulated molecules are sensitive to screening effects of the currents induced within the nanotube itself and that the

*Address correspondence to mk531@cam.ac.uk.

Received for review September 29, 2010 and accepted December 10, 2010.

Published online December 20, 2010.
10.1021/nn102590b

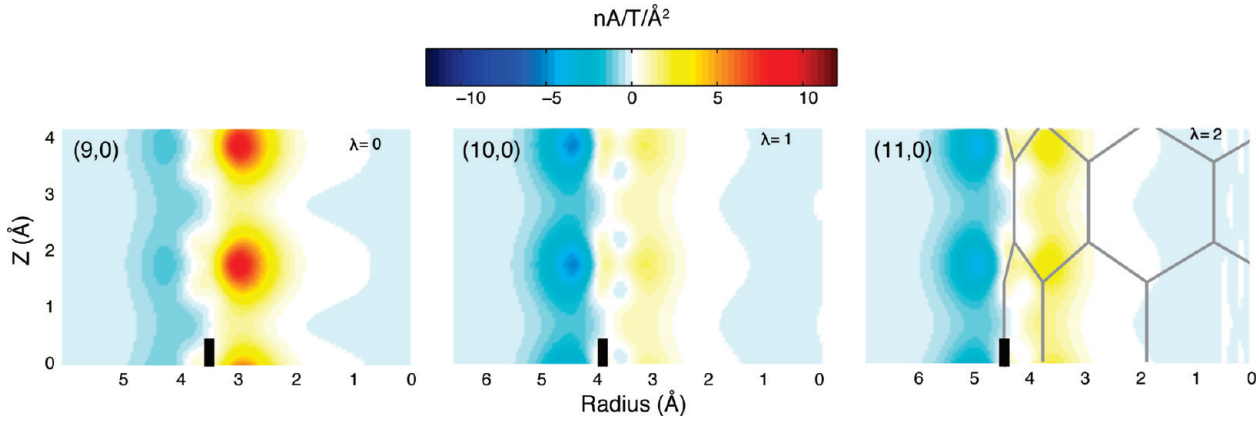

Figure 1. Magnetic-field-induced current densities for (9,0), (10,0), and (11,0) nanotubes, which correspond to nanotube families with λ = 0, 1, and 2, respectively. The radius of each nanotube is indicated by a black line on the *x* axis. The bonding network of the (11,0) nanotube has been superimposed onto the current density plot to aid the eye. A detailed description of the surface on which each current density is plotted can be found in the Methods and Computational Details section.

differences in chemical shifts between the encapsulated molecule and the free molecule could be used to identify the host nanotube using solid-state NMR experiments.

RESULTS AND DISCUSSION

Magnetically Induced Currents. Nanotubes can be divided into three families defined by the parameter λ = mod(*n*−*m*,3), where *n* and *m* are the nanotube chiral vectors (*n*,*m*). We focus on nonmetallic zigzag nanotubes of type (*n*,0). We first consider a magnetic field applied parallel to the nanotube axis, which will be taken as the *z* axis. For nanotubes where *n* = 9, 10, and 11, the cross sections of the induced current density are shown in Figure 1. These plots represent the typical behavior of the induced currents for zigzag nanotubes in each nanotube family. The detailed current topology is rather complex with currents flowing around the bonds but also moving in and out of the surface of the nanotube and around the atoms. The plots in Figure 1 show the general pattern of induced currents, and it can be seen that there is a positive (paramagnetic) current flow with respect to the tube axis on the inside of the tube and a negative (diamagnetic) current flow on the outside.[25] However, for the larger diameter λ = 0 nanotubes, where *n* = 12, 15, and 18, a positive current also flows on the outside of the tube. Current flow in the (15,0) nanotube is shown in Figure 4. When the magnetic field is applied perpendicular to the nanotube axis, in either the *x* or the *y* direction, the overall induced current is diamagnetic. In practice, we would expect currents at the edges of a nanotube to be different from those predicted for the bulk by our fully periodic model. These edge effects could lead to the broadening of the measured NMR spectra; however, these are expected to be localized at the edges and not affect the majority of the nanotube.

The total current circulating around the nanotube axis was computed by integrating the current density (details are given in the Methods and Computational Details section). The results are summarized in Table 1. Positive overall current corresponds to a net paramagnetic response and negative overall current to a net diamagnetic response. The λ = 0 nanotubes have an overall positive current flow, indicating a paramagnetic response, whereas the λ = 1 and 2 nanotubes have an overall negative current flow, indicating a diamagnetic response.[21,26] Recent NMR studies of encapsulated molecules[22,27] would be guided by consideration of these induced currents that affect the measured NMR parameters.

In each family of nanotubes, the magnitude of the current increases with the diameter of the tube; this increase is most rapid for the λ = 0 tubes. The variation of the total current with nanotube diameter is plotted in Figure 2a, where a trend is observed for the total current to tend to a constant for larger diameter tubes. We note that properties of nanotubes typically tend to those of graphene with increasing tube diameter. As our results show, this is not the case for the NMR re-

TABLE 1. Diameter (Å), Total Current (nA/T/Unit Cell), *z*-Component of the NICS (ppm), Isotropic NICS (ppm), and ^{13}C Isotropic Shieldings (ppm) for Infinitely Long *n* = 6−18 Zigzag Nanotubes (*n*,0)[a]

	D (Å)	current (nA/T/unit cell)	*z*-NICS (ppm)	iso-NICS (ppm)	^{13}C σ_{iso} (ppm)
(6,0)	4.8	3.7	13.5	−12.1	48.6
(9,0)	7.1	11.2	33.3	−5.5	44.4
(12,0)	9.5	16.3	45.6	−1.2	46.6
(15,0)	11.8	20.2	54.9	2.0	46.8
(18,0)	14.1	22.3	59.0	4.8	46.6
(7,0)	5.6	−4.3	−8.9	−10.8	29.6
(10,0)	7.9	−5.2	−12.1	−18.2	38.5
(13,0)	10.3	−5.4	−12.5	−20.2	42.4
(16,0)	12.6	−5.4	−12.5	−21.1	44.6
(8,0)	6.4	−1.6	−1.7	−18.0	34.7
(11,0)	8.7	−2.5	−4.8	−20.6	41.1
(14,0)	11.0	−3.0	−6.2	−21.5	44.0
(17,0)	13.4	−3.3	−7.0	−22.0	45.8

[a]Results are arranged in the order of nanotube families, first λ = 0, then 1 and 2.

sponse as the tubes always enclose an amount of magnetic flux.

The isotropic ^{13}C chemical shieldings for the nanotubes are presented in Table 1. These agree well with previous results for infinite nanotubes.[28] The differences in isotropic shieldings as compared to previous calculations result from a higher degree of convergence in the present work due to finer sampling of the Brillouin zone and from the use of a cylindrical sample shape for determining the macroscopic susceptibility contribution (see the Methods and Computational Details section for details). It should be noted that the larger diameter $\lambda = 0$ nanotubes are computed to have exceptionally small band gaps, and so, in practice, we would expect their NMR response to contain a contribution from the electronic spin, namely, a Knight shift.[29,30]

Molecule Encapsulation. Recent studies have examined the encapsulation of hydrogen,[8] xenon,[31] metal halides,[9] and water[32] in nanotubes as well as larger molecules, such as Buckminster fullerenes,[10] DNA,[11,33] and even proteins.[12,34] With the increasing purity and quality of carbon nanotube production, it is expected that the accuracy in the measurement of NMR parameters for encapsulated systems will increase. One of the first experimental NMR studies of molecule encapsulation in nanotubes indicates changes in isotropic chemical shifts as large as −68.3 ppm due to encapsulation.[22]

Recently, Besley and Noble[35] discussed the change in the chemical shift that occurs for a small molecule when it is placed inside a nanotube. They performed calculations on several small molecules, first isolated, and then positioned inside a variety of finite nanotubes. The observed change in the calculated shift will arise from a combination of local changes in the electronic structure of the molecules upon encapsulation or from the nonlocal effect of the currents flowing in the nanotube. To separate and, hence, quantify these effects, we compute the nucleus-independent chemical shift (NICS)[36] within the interior of infinitely periodic tubes.

Nucleus-Independent Chemical Shift. The NICS is a rank-2 tensor that gives the induced magnetic field for a given direction of the applied field. For a magnetic field applied along the *z* axis of a nanotube, the induced field at the center of the tube will, by symmetry, point along the tube axis and relate linearly to the *z*-component of the NICS (*z*-NICS). In Figure 3, we plot the *z*-NICS against the induced current for the 13 nanotubes studied here. There is close agreement between these calculated values and the expression obtained by assuming that the total induced current flows uniformly in a cylindrical shell (*i.e.*, a solenoid where $\mathbf{B}_{in} = \mu_0\mathbf{I}$).

On the time scales relevant to NMR experiments, a mobile encapsulated molecule would sample a large region inside the nanotube. To assess the impact of this sampling on the NMR response, we now consider the spatial variation of the induced field inside the tube. We first discuss the *z*-component of the NICS—for an ideal solenoid, we would find a uniform induced field—and then consider the isotropic NICS (iso-NICS).

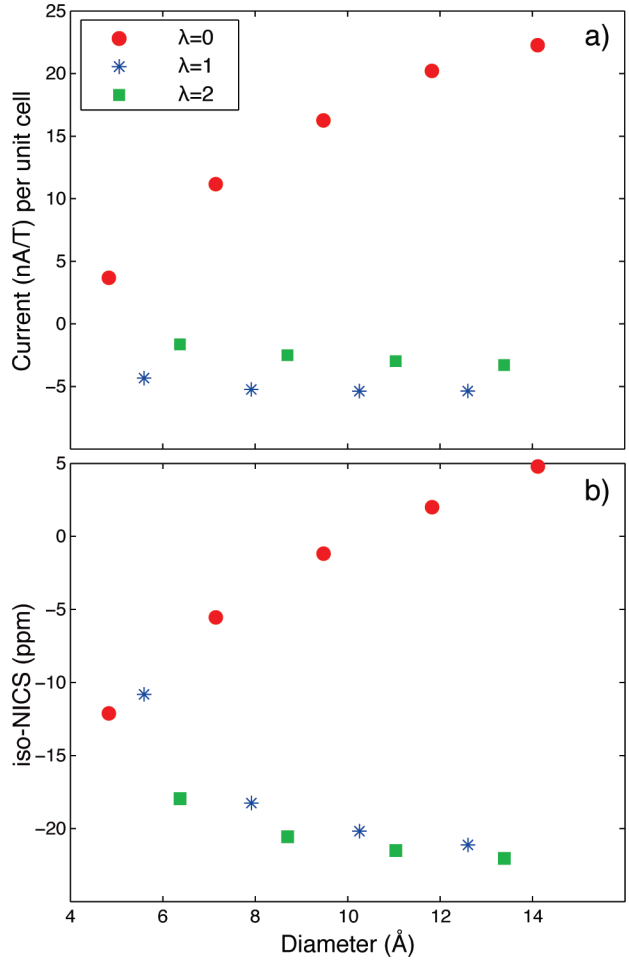

Figure 2. Variation of (a) the total magnetically induced current (nA/T/unit cell) and (b) the isotropic NICS with nanotube diameter (Å) for the three families of zigzag single-walled nanotubes.

To give a qualitative comparison, we discuss in detail the results for two nanotubes, $n = 10$ and 15. A

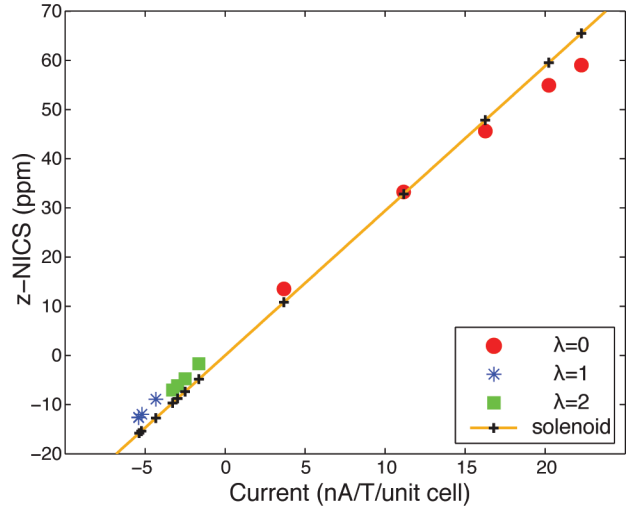

Figure 3. Comparison of the induced current in each nanotube *vs* the *z*-component of the NICS to that of a classical solenoid model $\mathbf{B}_{in} = \mu_0\mathbf{I}$, where I is the current per unit length.

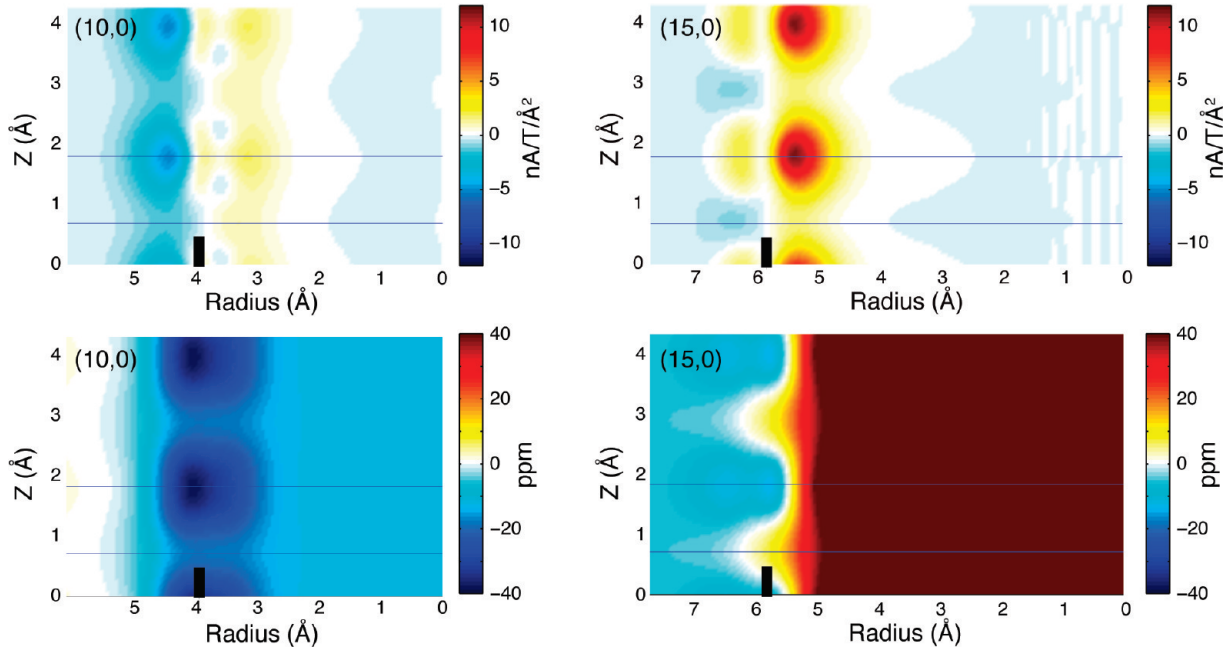

Figure 4. In the upper half of the figure, the two plots show the induced current densities for the (10,0) and (15,0) nanotubes. In the lower half, the two plots show the *z*-component of the NICS induced by these currents. The radius of each nanotube is indicated by a black line on the *x* axis.

cross section of the current density for the $n = 10$ nanotube and the $n = 15$ nanotube can be seen in the upper two plots in Figure 4. For the $n = 10$ tube, the plot shows a typical $\lambda = 1$ current density with an overall diamagnetic current flow of -5.2 nA/T/unit cell. For the $n = 15$ tube, the current flow is positive inside the tube and for some regions on the outside of the tube with an overall paramagnetic current of 20.2 nA/T/unit cell. The *z*-NICS induced by these currents is plotted in the two plots in the lower half of Figure 4. The *z*-NICS relates directly to the *z*-component of the induced magnetic field and thus, shows how the *z*-component of a magnetic field changes within the nanotube. The magnetic field varies in the vertical direction because the ring currents are quite distinct and vertically separated. However, it is clear that there is an inner region within each tube where the induced field is essentially constant. We can also see that the magnetic field changes across the $x-y$ plane. In Figure 5, the *z*-NICS is plotted on $x-y$ planes at the two *z*-axis positions of $Z = 0.7$ and 1.8 Å, which correspond to the two horizontal lines in Figure 4.

The (10,0) nanotube has a negative *z*-NICS inside the tube, whereas the (15,0) nanotube has a positive *z*-NICS. These relate directly to the diamagnetic and paramagnetic current responses of these nanotubes. Although variation in the NICS can be seen close to the nanotube wall, a uniform NICS region exists within the nanotube. This uniform region extends across the middle of the tube up to a radius of 2 Å for the $n = 10$ tube and a radius of 3 Å for the $n = 15$ nanotube. In these regions, *z*-NICSs are constant to within 0.5 ppm.

Our calculations of the *z*-NICS, a measure of the induced magnetic field inside the nanotubes due to the circulating currents, are highly relevant to any NMR analysis of molecule encapsulation in SWNTs. Another direct observable by the experiment on the effect of the induced currents and, thus, the effect of the *z*-NICS would be the value for the isotropic NICS inside the nanotubes. The variation of the iso-NICS calculated in the middle of each tube (Table 1) with the nanotube diameter is plotted in Figure 2b. The trend is for he isotropic NICS to increase with the diameter of the tube. We consider spatial variation of iso-NICS within the nanotubes in Figure 6, where we present the iso-NICS plotted on $x-y$ planes at $Z = 0.7$ and 1.8 Å for the $n = 10$ and 15 tubes, respectively. A region of almost uniform iso-NICS inside the nanotubes is, once again, evident. For the $n = 10$ nanotube, the region within a radius of 2 Å from the center of the tube has a variation in the iso-NICS of less than 0.5 ppm. For the $n = 15$ nanotube, the region within a radius of 4 Å from the center has a variation in the iso-NICS of less than 0.5 ppm.

Recently, Sebastiani and Kudin[37] have presented similar NICS plots for achiral and chiral carbon nanotubes. They predict much larger values for the isotropic NICS inside zigzag nanotubes, which appear to increase linearly with the diameter of the nanotube. We discuss the different approaches and possible reasons for the differences in the Methods and Computational Details section.

Computed Encapsulations. We now investigate the effect of magnetically induced currents and the corresponding NICS on encapsulated molecules by performing calculations for the isotropic chemical shifts on isolated

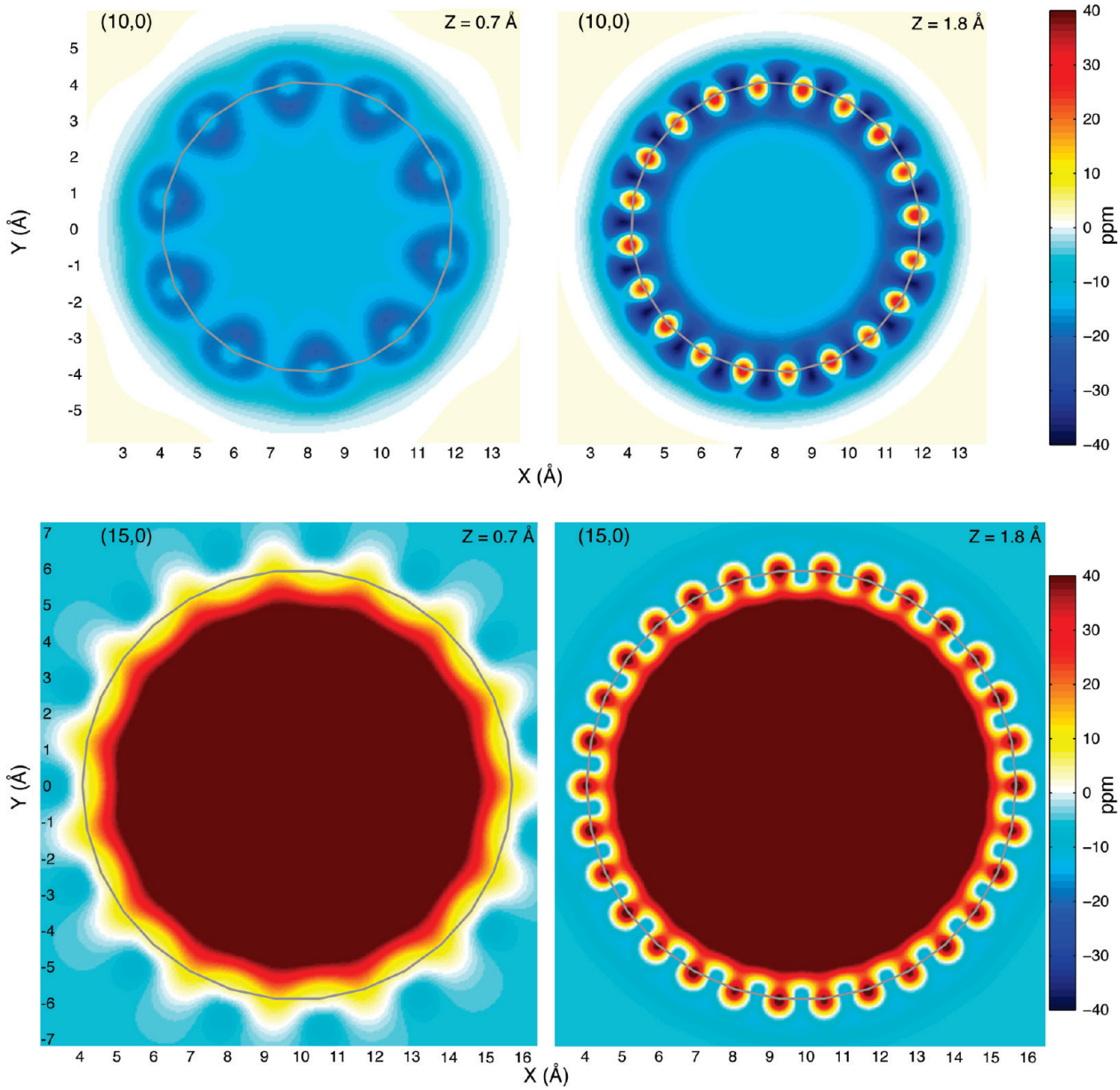

Figure 5. *z*-Component of the NICS for the (10,0) and the (15,0) nanotubes plotted on two *x*−*y* planes at the two different heights indicated in Figure 4. The locations of the nanotube walls are indicated by the gray line.

He, CH_4,and HCl molecules and the same molecules placed inside an infinite (9,0) nanotube. The results are presented in Table 2. So long as there is no interaction between the encapsulated molecule and the nanotube wall, the change in chemical shift due to encapsulation would arise solely from the orbital currents induced in the nanotube. In our calculations, we assume that, on encapsulation, the structure of the small molecule does not change; we would then expect the molecule's isotropic chemical shift on encapsulation to change by the iso-NICS value. However, similar calculations, including structural relaxations, could be used to relate chemical shifts to nanotube geometry for strongly bound encapsulated molecules. For applications where temporary encapsulation is required using weakly bound encapsulated molecules would be preferred as they are much easier to remove. For other technological applications, the identification using strongly bound encapsulated molecules may be a preferred route.

TABLE 2. Change in Isotropic Shift (Δiso) in Parts per Million Predicted by the Calculated Values of iso-NICS in the (9,0) Nanotube Compared to Calculated Changes in Isotropic Shifts for He, CH_4, and HCl Molecules[a]

		CH_4		HCl		
	He	H	C	H	Cl	iso-NICS
Δiso (ppm)	−5.0	−4.3	−3.6	−5.0	4.9	−5.5

[a]For the CH_4 molecule, the mean change in chemical shift for the four H atoms is presented.

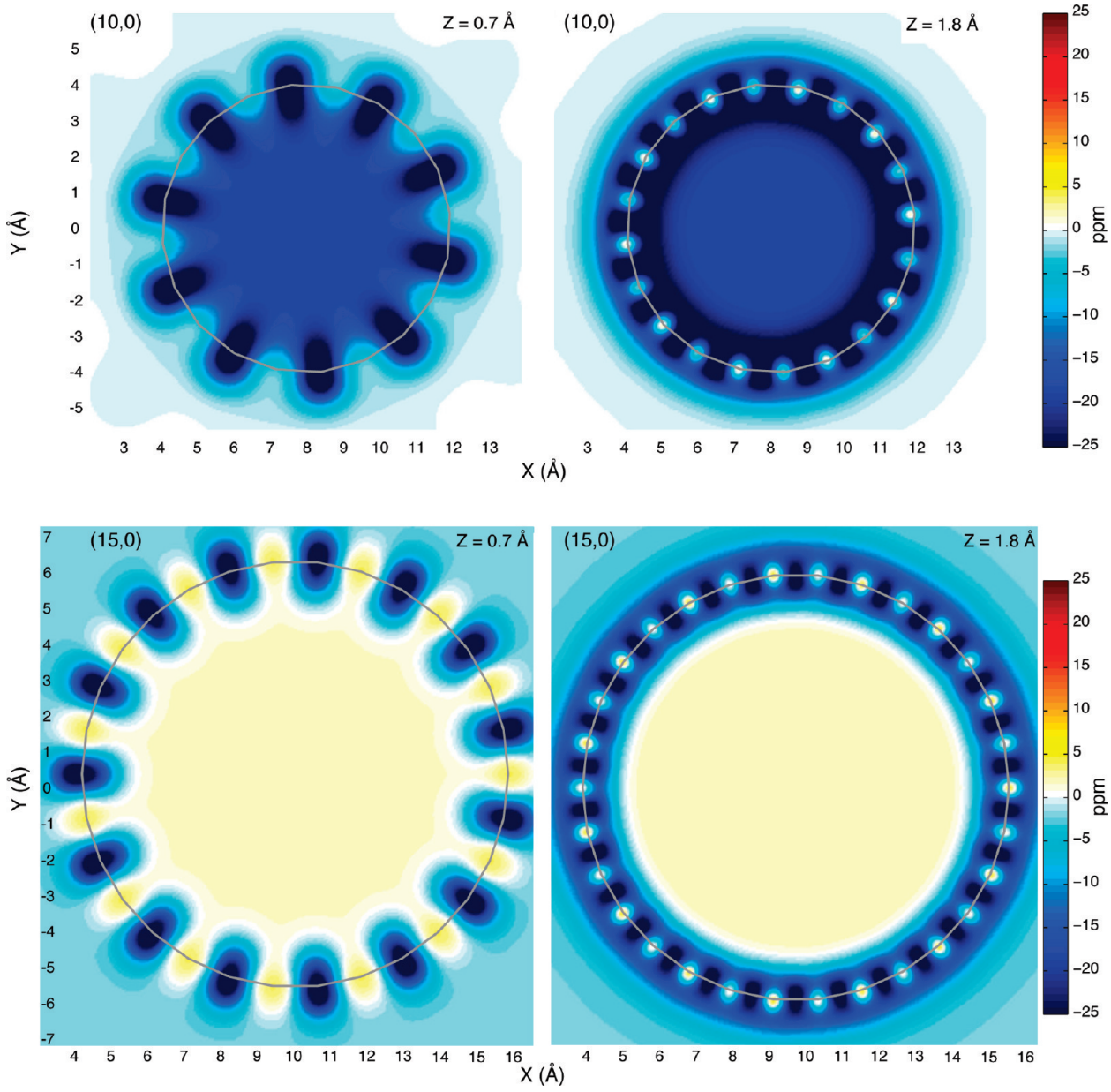

Figure 6. Isotropic NICS for the (10,0) and the (15,0) nanotubes plotted on two *x*−*y* planes at the two different heights indicated in Figure 4. The locations of the nanotube walls are indicated by the gray line.

The change in isotropic chemical shift between an isolated He atom and a He atom inside a (9,0) nanotube was calculated to be −5 ppm. The iso-NICS calculated in the middle of the (9,0) tube is −5.5 ppm, which clearly accounts for the majority of change in the isotropic shift (Δiso) for the He atom.

For CH_4, the situation is similar. The change in the isotropic chemical shift on encapsulation for the H atom lying on the axis of the nanotube (in line with the C atom) was −4.7 ppm. For the remaining three H atoms oriented toward the nanotube walls, the change in the chemical shift was −4.2 ppm. For the C atom, the change was −3.6 ppm. Again, these values are to be compared to the iso-NICS in the middle of the nanotube, which is −5.5 ppm. The calculated Δiso shifts are larger than the iso-NICS fluctuations in the central region of the tube and so must arise from an interaction with the tube wall.

For the HCl molecule, we calculate Δiso = −5.0 ppm for the H atom, but for the Cl atom, the calcu-

TABLE 3. Change in Isotropic Shift (Δiso) in Parts per Million Predicted by the Calculated Values of iso-NICS in (10,0), (11,0), (12,0), and (13,0) Nanotubes Compared to Calculated Changes in Isotropic Shifts for the HCl Molecule

	HCl		
	H	Cl	iso-NICS
(10,0)	−18.0	−13.7	−18.2
(11,0)	−20.4	−20.0	−20.6
(12,0)	−1.8	−2.1	−1.2
(13,0)	−20.1	−20.5	−20.2

lated change is +4.9 ppm. To investigate this unexpected behavior further, we placed a HCl molecule inside (10,0), (11,0), (12,0), and (13,0) tubes. The results are summarized in Table 3. In all these nanotubes, Δiso for H was accounted for by the iso-NICS of the tubes. For Cl, however, the expected change in the chemical shift was observed only in the larger nanotubes, (11,0), (12,0), and (13,0). The results show that, for smaller tubes, interactions with the nanotube walls can be present, however, for bigger tubes, such as (11,0), (12,0), and (13,0), the entire change in the isotopic shift for the Cl atom in the HCl molecule can be explained by the calculated iso-NICS.

We consider our encapsulation results to be more realistic than those of Besley and Noble,[35] who use short finite hydrogen-capped nanotubes as their model system. For such short nanotubes, the band gap is very small, and our infinite periodic models should provide a better description of real nanotubes.[38]

CONCLUSION

We have investigated magnetically induced currents in infinite single-walled carbon nanotubes of type (*n*,0) for $n = 6-18$. We conclude that the $\lambda = 0$ infinite nanotubes have an overall positive induced current, indicating a paramagnetic response, whereas the $\lambda = 1$ and 2 nanotubes with an overall negative induced current show a diamagnetic response.[21,26] In each family of nanotubes, the magnitude of the current increases with the tube diameter; this increase is faster for the $\lambda = 0$ tubes.

We also computed the NICS inside these nanotubes. The *z*-component of the NICS, which is induced by the current flow around the nanotube, was found to agree closely with a simple classical solenoid model. Both the *z*-component and the isotropic NICS inside the larger nanotubes showed a large uniform region around the center of the tube where, for example, a molecule could be encapsulated. A large difference in NICS was found between different nanotubes. This would lead to different changes in the chemical shifts of a molecule encapsulated inside different nanotubes. This change in chemical shift is large and experimentally significant. This opens up the possibility of characterizing nanotubes by measuring the change in the chemical shifts of encapsulated molecules.

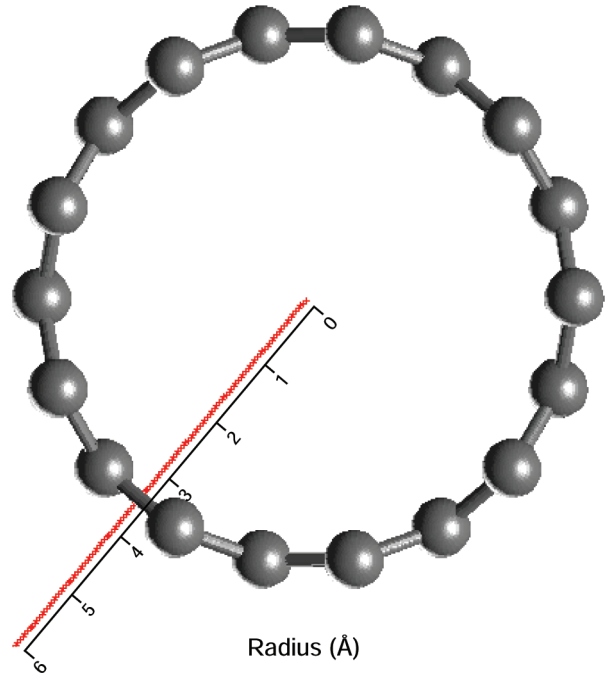

Figure 7. Top view of the 2D grid (red) of points used for the calculation of the total current.

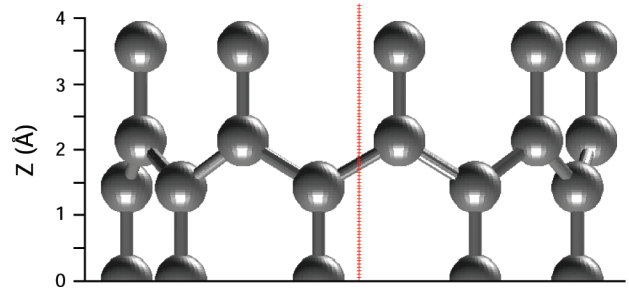

Figure 8. Side view of the 2D grid (red) of points used for the calculation of the total current.

METHODS AND COMPUTATIONAL DETAILS

Nanotubes are divided into three families defined by the parameter $\lambda = \mathrm{mod}(n-m,3)$, where *n* and *m* are the nanotube chiral vectors (*n*,*m*). We focus on nonmetallic zigzag nanotubes of type (*n*,0). The geometries for the $n = 9-17$ isolated nanotubes were taken directly from Zurek *et al.*[28] The $n = 6$ and 18 nanotubes were generated using the TUBEGEN[39] tool, and their geometry was optimized through first-principles using parameters similar to those used in ref 28.

Magnetic shielding tensors were calculated for each isolated infinite single-walled nanotube using the gauge including projector augmented wave (GIPAW)[40] approach implemented in the CASTEP code.[41] This approach is capable of treating periodic systems and can also be applied to finite systems using a supercell technique. The CASTEP code uses a plane-wave basis set implementation of density-functional theory. Calculations were carried out using ultrasoft pseudopotentials[42] with the Perdew–Burke–Ernzerhof[43] exchange-correlation functional and a maximum plane-wave energy of 500 eV. As found in previous studies,[28] this energy cut off was found to be sufficient to converge isotropic chemical shifts.

In the GIPAW approach, the total current is divided into contributions from the core states of the atoms, the pseudised valence electrons, and atom centered augmentation terms, which account for the difference between the pseudo and true all-electron states close to the nucleus.[44] To obtain the chemical shielding tensor, we must include all the contributions to the current. However, to visualize the induced current, we focus on the current from the pseudised valence electrons as this will be the only contribution in the region away from the nucleus. Within the plane-wave calculations, this current is calculated in real space on a regular grid in the unit cell. We use Fourier interpolation to calculate the current on an arbitrary grid,[45] in our case, a grid that cuts the carbon bonds in the nanotubes. This

grid is used to visualize the current density across the nanotubes. If we look at this grid from the top, as can be seen in Figure 7, the grid is chosen such that it cuts the midpoint of the carbon bond. When the grid is viewed from the side, as in Figure 8, the grid cuts the bond at an angle.

The magnetic shielding tensor is calculated from the induced current using the Biot−Savart Law

$$\mathbf{B}^{(1)}_{\text{in}}(\mathbf{r}) = \frac{1}{c}\int d^3r' \mathbf{j}^{(1)}(\mathbf{r}') \times \frac{\mathbf{r} - \mathbf{r}'}{|\mathbf{r} - \mathbf{r}'|^3} \quad (1)$$

The linearity of eq 1 allows us to calculate the induced magnetic field from each current contribution independently.[40] For the bare current contribution, the Biot−Savart Law is applied in reciprocal space

$$\mathbf{B}^{(1)}_{\text{bare}}(\mathbf{G}) = \frac{4\pi}{c}\frac{i\mathbf{G} \times \mathbf{j}^{(1)}_{\text{bare}}(\mathbf{G})}{G^2} \quad (2)$$

and the induced magnetic field at position **R** is obtained by an explicit Fourier transform

$$\mathbf{B}^{(1)}_{\text{bare}}(\mathbf{R}) = \sum_{\mathbf{G}} e^{i\mathbf{G}\cdot\mathbf{R}}\mathbf{B}^{(1)}_{\text{bare}}(\mathbf{G}) \quad (3)$$

The three contributions are summed to get the total induced magnetic field. The chemical shielding tensor, σ, is then calculated from

$$\sigma(\mathbf{R}) = -\frac{\mathbf{B}_{\text{in}}(\mathbf{R})}{\mathbf{B}_0} \quad (4)$$

For a bulk material, the chemical shielding contains a contribution $\sigma(\mathbf{G} = 0)$ that depends on the shape of the sample.[46] We follow Marques *et al.*[21] and present results for a cylindrical sample shape. Note that the current within the unit cell is independent of this choice.

For each nanotube structure, the isotropic shielding σ_{iso} was calculated from the diagonalized symmetric part of the magnetic shielding tensor

$$\sigma_{\text{iso}} = \frac{1}{3}(\sigma_{11} + \sigma_{22} + \sigma_{33}) \quad (5)$$

The isotropic chemical shift has the same magnitude, but the opposite sign, as the isotropic shielding. To calculate the principal components of the nucleus-independent chemical shift (NICS),[36] we simply use the negative value of eq 4 at non-nuclear positions. We then use the *z*-component of the NICS (*z*-NICS) to relate the effect of the induced magnetic field inside the nanotube and the average of the three components as the isotropic NICS (iso-NICS) to provide predictions of the change in isotropic chemical shifts for encapsulated molecules within each tube. Previous studies on nanotubes have demonstrated the need for extremely fine sampling of the Brillouin zone in order to obtain accurate NMR parameters.[28] This is particularly true in the case of the small-band-gap $\lambda = 0$ tubes. The Brillouin zone was sampled using a Monkhorst−Pack[47] *k*-point grid of dimension (1,1,*q*) with *q* chosen to achieve convergence to a high accuracy. All the chemical shifts were converged to within 1 ppm. For this, it was necessary to vary *q* between 96 and 512 depending on the nanotube band gap, the higher values being necessary for the small-band-gap tubes. The largest calculation we performed was on an (18,0) nanotube. The unit cell contained 72 carbon atoms, and the Brillouin zone was sampled with 512 *k*-points. We obtain values of the NICS that tend toward a limit with increasing nanotube diameter. This is contrary to the previous results of Sebastiani and Kudin.[37] We note that their method is restricted to Brillouin zone sampling at the Γ-point and convergence approached by increasing the length of the tube. Given the very fine *k*-point sampling we need to achieve convergence, we suggest that this may be the origin of their different results.

All visualizations were done using Matlab and the Adobe CS3 Package.

Acknowledgment. We thank C. J. Pickard for useful interactions. Computing resources were provided by the Cambridge High Performance Computing Service HPCS and were funded by EPSRC under Grant No. EP/F032773/1 and the Royal Society.

REFERENCES AND NOTES

1. Dresselhaus, M. S.; Dresselhaus, G.; Saito, R.; Jorio, A. Raman Spectroscopy of Carbon Nanotubes. *Phys. Rep.* **2005**, *409*, 47–99.
2. Arnold, M. S.; Green, A. A.; Hulvat, J. F.; Stupp, S. I.; Hersam, M. C. Sorting Carbon Nanotubes by Electronic Structure Using Density Differentiation. *Nat. Nanotechnol.* **2006**, *1*, 60–65.
3. Khlobystov, A. N.; Britz, D. A.; Briggs, G. A. D. Molecules in Carbon Nanotubes. *Acc. Chem. Res.* **2005**, *38*, 901–909.
4. Britz, D. A.; Khlobystov, A. N. Noncovalent Interactions of Molecules with Single Walled Carbon Nanotubes. *Chem. Soc. Rev.* **2006**, *35*, 637–659.
5. Zhao, M. W.; Xia, Y. Y.; Ma, Y. C.; Ying, M. J.; Liu, X. D.; Mei, L. M. Exohedral and Endohedral Adsorption of Nitrogen on the Sidewall of Single-Walled Carbon Nanotubes. *Phys. Rev. B* **2002**, *66*, 155403.
6. Zhao, M. W.; Xia, Y. Y.; Lewis, J. P.; Mei, L. M. Chemical Reactivity of Single-Walled Carbon Nanotubes to Amidogen from Density Functional Calculations. *J. Phys. Chem. B* **2004**, *108*, 9599–9603.
7. Chen, Z. F.; Thiel, W.; Hirsch, A. Reactivity of the Convex and Concave Surfaces of Single-Walled Carbon Nanotubes (SWCNTs) Towards Addition Reactions: Dependence on the Carbon-Atom Pyramidalization. *ChemPhysChem* **2003**, *4*, 93.
8. Mpourmpakis, G.; Froudakis, G. E.; Lithoxoos, G. P.; Samios, J. Effect of Curvature and Chirality for Hydrogen Storage in Single-Walled Carbon Nanotubes: A Combined Ab Initio and Monte Carlo Investigation. *J. Chem. Phys.* **2007**, *126*, 10.
9. Hong, S. Y.; Tobias, G.; Al-Jamal, K. T.; Ballesteros, B.; Ali-Boucetta, H.; Lozano-Perez, S.; Nellist, P. D.; Sim, R. B.; Finucane, C.; Mather, S. J.; et al. Filled and Glycosylated Carbon Nanotubes for In Vivo Radioemitter Localization and Imaging. *Nat. Mater.* **2010**, *9*, 485–90.
10. Smith, B. W.; Monthioux, M.; Luzzi, D. E. Encapsulated C60 in Carbon Nanotubes. *Nature* **1998**, *396*, 323–324.
11. Gao, H. J.; Kong, Y.; Cui, D. X.; Ozkan, C. S. Spontaneous Insertion of DNA Oligonucleotides into Carbon Nanotubes. *Nano Lett.* **2003**, *3*, 471–473.
12. Tsang, S. C.; Davis, J. J.; Green, M. L. H.; Allen, H.; Hill, O.; Leung, Y. C.; Sadler, P. J. Immobilization of Small Proteins in Carbon Nanotubes—High-Resolution Transmission Electron-Microscopy Study and Catalytic Activity. *J. Chem. Soc., Chem. Commun.* **1995**, 1803–1804.
13. Douglas, T.; Young, M. Host-Guest Encapsulation of Materials by Assembled Virus Protein Cages. *Nature* **1998**, *393*, 152–155.
14. Bianco, A.; Kostarelos, K.; Partidos, C. D.; Prato, M. Biomedical Applications of Functionalised Carbon Nanotubes. *Chem. Commun.* **2005**, 571–577.
15. Bianco, A.; Kostarelos, K.; Prato, M. Applications of Carbon Nanotubes in Drug Delivery. *Curr. Opin. Chem. Biol.* **2005**, *9*, 674–679.
16. Hilder, T. A.; Hill, J. M. Modeling the Loading and Unloading of Drugs into Nanotubes. *Small* **2009**, *5*, 300–308.
17. Hilder, T. A.; Hill, J. M. Modelling the Encapsulation of the Anticancer Drug Cisplatin into Carbon Nanotubes. *Nanotechnology* **2007**, *18*, 8.
18. Hilder, T. A.; Hill, J. M. Probability of Encapsulation of Paclitaxel and Doxorubicin into Carbon Nanotubes. *Micro Nano Lett.* **2008**, *3*, 41–49.
19. Kang, Y.; Wang, Q.; Liu, Y. C.; Wu, T.; Chen, Q.; Guan, W. J. Dynamic Mechanism of Collagen-like Peptide Encapsulated into Carbon Nanotubes. *J. Phys. Chem. B* **2008**, *112*, 4801–4807.
20. Tang, X. P.; Kleinhammes, A.; Shimoda, H.; Fleming, L.; Bennoune, K. Y.; Sinha, S.; Bower, C.; Zhou, O.; Wu, Y.

Electronic Structures of Single-Walled Carbon Nanotubes Determined by NMR. *Science* **2000**, *288*, 492–494.
21. Marques, M. A. L.; d'Avezac, M.; Mauri, F. Magnetic Response and NMR Spectra of Carbon Nanotubes from Ab Initio Calculations. *Phys. Rev. B* **2006**, *73*, 125433.
22. Kim, Y.; Abou-Hamad, E.; Rubio, A.; Wagberg, T.; Talyzin, A. V.; Boesch, D.; Aloni, S.; Zettl, A.; Luzzi, D. E.; Goze-Bac, C. Communications: Nanomagnetic Shielding: High-Resolution NMR in Carbon Allotropes. *J. Chem. Phys.* **2010**, *132*, 021102.
23. Shaver, J.; Parra-Vasquez, A. N. G.; Hansel, S.; Portugall, O.; Mielke, C. H.; von Ortenberg, M.; Hauge, R. H.; Pasquali, M.; Kono, J. Alignment Dynamics of Single-Walled Carbon Nanotubes in Pulsed Ultrahigh Magnetic Fields. *ACS Nano* **2009**, *3*, 131–138.
24. Searles, T. A.; Imanaka, Y.; Takamasu, T.; Ajiki, H.; Fagan, J. A.; Hobbie, E. K.; Kono, J. Large Anisotropy in the Magnetic Susceptibility of Metallic Carbon Nanotubes. *Phys. Rev. Lett.* **2010**, *105*, 017403.
25. Lazzeretti, P. Ring Currents. *Prog. Nucl. Magn. Reson. Spectrosc.* **2000**, *36*, 1–88.
26. López-Urías, F.; Rodríguez-Manzo, J. A.; Muñoz Sandoval, E.; Terrones, M.; Terrones, H. Magnetic Response in Finite Carbon Graphene Sheets and Nanotubes. *Opt. Mater.* **2006**, *29*, 110–115.
27. Abou-Hamad, E.; Kim, Y.; Wagberg, T.; Boesch, D.; Aloni, S.; Zettl, A.; Rubio, A.; Luzzi, D. E.; Goze-Bac, C. Molecular Dynamics and Phase Transition in One-Dimensional Crystal of C-60 Encapsulated Inside Single Wall Carbon Nanotubes. *ACS Nano* **2009**, *3*, 3878–3883.
28. Zurek, E.; Pickard, C. J.; Walczak, B.; Autschbach, J. Density Functional Study of the C-13 NMR Chemical Shifts in Small-to-Medium-Diameter Infinite Single-Walled Carbon Nanotubes. *J. Phys. Chem. A* **2006**, *110*, 11995–12004.
29. Knight, W. D. Nuclear Magnetic Resonance Shift in Metals. *Phys. Rev.* **1949**, *76*, 1259–1260.
30. Yazyev, O. V.; Helm, L. Isotropic Knight Shift of Metallic Carbon Nanotubes. *Phys. Rev. B* **2005**, *72*, 245416.
31. Clewett, C. F. M.; Pietrass, T. Xe-129 and Xe-131 NMR of Gas Adsorption on Single- and Multi-Walled Carbon Nanotubes. *J. Phys. Chem. B* **2005**, *109*, 17907–17912.
32. Mao, S. H.; Kleinhammes, A.; Wu, Y. NMR Study of Water Adsorption in Single-Walled Carbon Nanotubes. *Chem. Phys. Lett.* **2006**, *421*, 513–517.
33. Ito, T.; Sun, L.; Crooks, R. M. Observation of DNA Transport Through a Single Carbon Nanotube Channel using Fluorescence Microscopy. *Chem. Commun.* **2003**, 1482–1483.
34. Chen, Q.; Wang, Q.; Liu, Y. C.; Wu, T.; Kang, Y.; Moore, J. D.; Gubbins, K. E. Energetics Investigation on Encapsulation of Protein/Peptide Drugs in Carbon Nanotubes. *J. Chem. Phys.* **2009**, *131*, 015101.
35. Besley, N. A.; Noble, A. NMR Chemical Shifts of Molecules Encapsulated in Single Walled Carbon Nanotubes. *J. Chem. Phys.* **2008**, *128*, 101102.
36. Schleyer, P. V.; Maerker, C.; Dransfeld, A.; Jiao, H. J.; Hommes, N. J. R. V. Nucleus-Independent Chemical Shifts: A Simple and Efficient Aromaticity Probe. *J. Am. Chem. Soc.* **1996**, *118*, 6317–6318.
37. Sebastiani, D.; Kudin, K. N. Electronic Response Properties of Carbon Nanotubes in Magnetic Fields. *ACS Nano* **2008**, *2*, 661–668.
38. Zurek, E.; Autschbach, J. Density Functional Calculations of the C-13 NMR Chemical Shifts in (9,0) Single-Walled Carbon Nanotubes. *J. Am. Chem. Soc.* **2004**, *126*, 13079–13088.
39. Frey, J.; Doren, D. J. *TubeGen 3.3*, http://turin.nss.udel.edu/research/tubegenonline.html, 2005.
40. Pickard, C. J.; Mauri, F. All-Electron Magnetic Response with Pseudopotentials: NMR Chemical Shifts. *Phys. Rev. B* **2001**, *63*, 13.
41. Clark, S. J.; Segall, M. D.; Pickard, C. J.; Hasnip, P. J.; Probert, M. J.; Refson, K.; Payne, M. C. First Principles Methods using CASTEP. *Z. Kristallogr.* **2005**, *220*, 567–570.
42. Yates, J. R.; Pickard, C. J.; Mauri, F. Calculation of NMR Chemical Shifts for Extended Systems using Ultrasoft Pseudopotentials. *Phys. Rev. B* **2007**, *76*, 024401.
43. Perdew, J. P.; Burke, K.; Ernzerhof, M. Generalized Gradient Approximations Made Simple. *Phys. Rev. Lett.* **1996**, *77*, 3865–3868.
44. Yates, J. R.; Pickard, C. J. Computations of Magnetic Resonance Parameters for Crystalline Systems: Principles. *Encyclopedia of Magnetic Resonance*; Harris, R. K.; Wasylishen, R. E., Eds.; John Wiley & Sons, Ltd.: Chichester, U.K., 2007.
45. Sebastiani, D. Current Densities and Nucleus-Independent Chemical Shift Maps from Reciprocal-Space Density Functional Perturbation Theory Calculations. *ChemPhysChem* **2006**, *7*, 164–175.
46. Mauri, F.; Pfrommer, B. G.; Louie, S. G. Ab Initio Theory of NMR Chemical Shifts in Solids and Liquids. *Phys. Rev. Lett.* **1996**, *77*, 5300–5303.
47. Monkhorst, H. J.; Pack, J. D. Special Points for Brillouin-Zone Integration. *Phys. Rev. B* **1976**, *13*, 5188.